Nonadiabatic quantum wave packet dynamics of H+H2 (HD) reactions

3 AUTHORS:

B. Jayachander Rao
University of Coimbra
12 PUBLICATIONS **51** CITATIONS

SEE PROFILE

Ramanathan Padmanaban
Pondicherry University
12 PUBLICATIONS **180** CITATIONS

SEE PROFILE

Susanta Mahapatra
University of Hyderabad
114 PUBLICATIONS **1,639** CITATIONS

SEE PROFILE

ELSEVIER

Nonadiabatic quantum wave packet dynamics of H + H₂ (HD) reactions

B. Jayachander Rao, R. Padmanaban, S. Mahapatra *

School of Chemistry, University of Hyderabad, Hyderabad 500 046, India

Abstract

Initial state-selected and energy resolved integral reaction cross sections and thermal rate constants of H + H₂ and H + HD reactions are calculated on the conically intersecting ground electronic manifold. The effect of the associated nonadiabatic coupling on these dynamical quantities is examined for energies upto the three-body dissociation limit well beyond the energetic minimum of the seam of conical intersections. The quantum dynamical simulations in the coupled electronic manifold are carried out within the coupled state approximation by a time-dependent wave packet propagation method employing the double many body expansion (DBME) potential energy surface (PES) of Varandas et al. [A.J.C. Varandas, F.B. Brown, C.A. Mead, D.G. Truhlar, N.C. Blais, J. Chem. Phys. 86 (1987) 6258]. All partial wave contributions upto the total angular momentum $J = 50$, in case of H + H₂ and $J = 60$, in case of H + HD reactions are considered to obtain converged reaction cross sections upto a total energy of ∼4.7 eV. Channel specific reaction cross sections are reported for the H + HD reaction. Analysis of the reaction probabilities for individual J values reveal no significant effect of nonadiabatic coupling on them at energies above the minimum of the seam of conical intersections occurring at ∼2.74 eV. The differences observed in the reaction probability results in the uncoupled and coupled surface situation however, cancel out in the integral reaction cross sections and thermal rate constants. These findings are consistent with the recent studies on these reactions including the geometric phase change.

© 2007 Elsevier B.V. All rights reserved.

1. Introduction

The H + H₂ reaction and its isotopic variants have been extensively studied both experimentally and theoretically during the last few decades [1]. Good agreement between the theory and experiment has been achieved in integral and differential reaction cross sections and thermal rate constants [2–15]. Due to the fact that these reactions take place on an orbitally degenerate electronic state and which is liable to the Jahn–Teller (JT) distortions, a study of the electronic nonadiabatic effects on their nuclear dynamics has been an important topic in recent years. The orbital degeneracy of H₃ (and its isotopomers) is split when it is distorted from its equilibrium D_{3h} configuration along its degenerate asymmetric stretching and bending vibrational

modes and belong to the well known $(E \otimes e)$-JT class of systems. The resulting two JT split component potential energy surfaces (PESs) form conical intersections (CIs) at the D_{3h} equilibrium configuration of these systems [16]. The lower adiabatic component of these two PESs is of repulsive type and forms pathways for the scattering processes. The effect of the conical intersections of this PES with the upper adiabatic PES on the H + H₂ (and its isotopic variants) reaction dynamics has been a debatable issue and is of immense current interest.

The effect of CIs on the reactive scattering dynamics of H + H₂ and its isotopic variants are well studied in the literature in terms of the geometric phase (GP) change of the adiabatic electronic wavefunction when encircling the CI in a closed path. In order to account for this phase change and to make the total wavefunction single valued, a vector potential is introduced into the nuclear Hamiltonian [17]. Early work on the GP effect in hydrogen exchange reaction

---

* Corresponding author. Fax: +91 40 23011537/23012460.
E-mail address: smsc@uohyd.ernet.in (S. Mahapatra).

was done by Mead [18], who showed that the GP changes the relative phases of the inelastic and reactive contributions to fully symmetrized cross sections. This was followed by extensive calculations by Kuppermann and co-workers [19], who performed pioneering quantum reactive scattering dynamics calculations of hydrogen exchange reaction and its isotopic variants for collision energies less than 2 eV. The GP effect was found to change markedly the state-to-state rovibrational product distributions [19], bringing them into better agreement with the early experimental measurements of these quantities [20]. However, subsequent comparisons of product state distributions and state-to-state differential cross sections obtained from calculations that omit the GP change [1,11,12,14,15], with the experimental results revealed an excellent agreement. This lead to some controversies and the issue remained debatable for quite sometime. Recently, Kendrick [21] performed a new set of accurate time-independent quantum reactive scattering calculations on the hydrogen exchange reaction and its isotopic variants, including the GP change using the vector potential approach. This author has computed the integral and differential reaction cross sections upto the total energy of ∼2.32 eV with and without including the GP change. The results of these calculations contradicted to those of Kuppermann and co-workers [19]. For a given value of the total angular momentum, J, the state-to-state reaction probabilities have been shown to exhibit a small but noticeable GP effects, which average out upon summing over all partial wave contributions to calculate the integral and differential reaction cross sections. The results of this study have been reconfirmed by Juanes-Marcos and Althorpe [22] by an entirely different theoretical approach. These authors have carried out time-dependent wave packet (WP) calculations with and without including the GP change. These authors obtained unequivocal agreement with the recent results of Kendrick [21], predicting GP effects in the state-to-state reaction probabilities, which cancel exactly on summing over the partial wave contributions in the integral reaction cross sections. Their findings are also consistent with those of Kendrick in predicting that there are no significant GP effects in the full differential cross sections at energies less than 1.8 eV, and in the partial differential cross sections at energies above this. But in addition to this, they also observed small GP effects in the full differential cross sections above 1.8 eV [22] (which was not reported by Kendrick) which may be experimentally observable. They also found that the small GP effects which are observed in the state-to-state reaction probabilities, are not observed in the integral reaction cross sections. The nuclear wavefunction around a CI has been shown to branch into an even and a odd component (with a sign change that depends on the geometric phase) and these two components can interfere and contribute to the partial cancellation of the GP effects in the reaction cross sections [23].

The GP change also shown to have only negligible effect on the transition state resonances in the H + H₂ collision

[24]. Due to the fact that the conical intersections occur at the D_{3h} equilibrium geometry of H_3, understandably the saddle point resonances (originating mainly from the collinear geometries) are not affected by the strong nonadiabatic effects. The direct evidence of the strong nonadiabatic effects in the H_3 system and its isotopic variants emerged from the neutralized ion-beam experiment of Bruckmeier et al. [25] which probed these systems in the vicinity of the intersection seams of their ground electronic manifold. In later theoretical studies and in conjunction with these experimental results, Mahapatra and Köppel [26] have unambiguously established the importance of the nonadiabatic coupling in the Rydberg emission spectra of these systems. In the recent past, Mahapatra et al. [27,28] have studied the role of CIs on the hydrogen exchange reaction on its conically intersecting ground electronic PES for $J = 0$ also for the first time. In this work, the authors have computed the initial state-selected total reaction probabilities for $J = 0$ by a time-dependent WP method by considering both the upper and lower adiabatic sheets and the nonadiabatic coupling between them. In this way the GP change and the nonadiabatic coupling are both included in the reaction dynamics in a consistent fashion. They have calculated the reaction probabilities for energies upto the onset of the three-body dissociation of H_3 and found a very minor impact of nonadiabatic coupling on the reaction dynamics for $J = 0$. In the present work this model is extended within the coupled states (CS) approximation to calculate the reaction cross sections and thermal rate constants and to elucidate the effect of nonadiabatic coupling on them. To the best of our knowledge the dynamical quantities for total energies upto the three-body dissociation limit, that is ∼2 eV above the minimum of the seam of the CIs have not been reported in the literature so far. Therefore, nonadiabatic effects, if at all, important for the dynamics of the H + H₂ reaction is expected to be revealed by the results of the present study extending to such high energies.

In the quantum dynamical simulations, we find that inclusion of partial wave contributions upto $J = 50$ is necessary to obtain the converged initial state-selected integral reaction cross sections upto the total energy close to the three-body dissociation limit in the H + H₂ and upto $J = 60$, in the H + HD reactions, respectively. These cross sections are calculated both in the coupled and uncoupled surface situations, and they show only minor differences beyond the minimum of the seam of CIs occurring at ∼2.74 eV. These findings are consistent with the single surface calculations reported in the literature including the GP change of the wavefunction [21,22]. It is important to note that the uncoupled surface calculations reported in this paper refer to the treatment of the nuclear dynamics on the lower adiabatic sheet only without inclusion of any nonadiabatic coupling and GP change. In the case of H + H₂ reaction, the cross section initially increase with increase in the total energy and reaches a maximum of ∼2.5 Å² at ∼2.5 eV and then decreases at higher energies.

The difference between the cross sections calculated with coupled and uncoupled surface situations somewhat increases with the rotational excitation of the reagent H_2. We also observe that the thermal rate constants computed in the coupled and uncoupled state situations differ only slightly. In case of H + HD reaction, the cross section initially increases with the total energy and reaches to a maximum of around ~1.6 Å² at ~3.5 eV and then decreases. In this case also, the thermal rate constants calculated in the coupled and uncoupled surface situations reveal only marginal difference.

This paper is aimed to elucidate the nonadiabatic coupling effects (which implicitly includes the GP effects) over a wide energy range (starting from the onset of the reaction to the three-body dissociation limit) in the H + H_2 (HD) reaction dynamics, and is organized in the following way. In Section 2, we present the theoretical formalism employed in this work. In Section 3, the computational details are outlined. In Section 4, we present the numerical results obtained on the H + H_2 and H + HD exchange reactions and discuss the effect of nonadiabatic coupling on them. Finally, the findings of the paper is summarized in Section 5.

2. Theoretical details

In this section we describe the theoretical formalism to calculate the initial state-selected and energy resolved reaction probabilities, integral reaction cross sections and thermal rate constants for the H + H_2 (HD) reactions. The reaction probabilities are calculated in the usual way, *i.e.,* from the expectation values of the quantum flux operator in the basis of the energy normalized time-independent reactive scattering wavefunction. The initial WP, $|\Psi(t = 0)\rangle$, pertinent to the reagents (H + H_2 or H + HD) is prepared in the asymptotic reagent channel when there is no interactions between the reagent atom and diatom. This WP is propagated in the coupled manifold of the electronic ground state of the respective systems by solving the time-dependent Schrödinger equation (TDSE) numerically on a grid. For an explicitly time-independent Hamiltonian (like in the present case), the solution reads

$$|\Psi(t)\rangle = \exp\left[\frac{-i\hat{H}t}{\hbar}\right]|\Psi(t = 0)\rangle, \tag{1}$$

where $|\psi(t)\rangle$ is the wavefunction of the reacting system at time t, and $\hat{H}$ defines the Hamiltonian operator of the collisional system.

2.1. The Hamiltonian

The interaction Hamiltonian in a diabatic basis of the ground electronic manifold of the H + H_2 (and its isotopomer H + HD) system can be written as

$$H^{\mathrm{d}} = T_N \begin{pmatrix} 1 & 0 \\ 0 & 1 \end{pmatrix} + \begin{pmatrix} U_{11} & U_{12} \\ U_{21} & U_{22} \end{pmatrix}, \tag{2}$$

where T_N represents the nuclear kinetic energy operator, which is diagonal in this basis. In terms of the mass-scaled body-fixed (BF) Jacobi coordinates R (the distance of the hydrogen atom to the center of mass of the diatomic reagent molecule), r (the internuclear distance of the reagent molecule) and γ (the angle between $\vec{R}$ and $\vec{r}$) and for total angular momentum $J \neq 0$, it is given by

$$T_N = -\frac{\hbar^2}{2\mu}\left[\frac{\partial^2}{\partial R^2} + \frac{\partial^2}{\partial r^2}\right] + \frac{\hat{j}^2}{2\mu r^2} + \frac{\hat{l}^2}{2\mu R^2}. \tag{3}$$

The quantities U_{11} and U_{22} in Eq. (2) are the energies of the two diabatic electronic states and, $U_{12} = U_{21}$ represent their coupling potential. The operator $\hat{j}$ defines the diatomic rotational angular momentum associated with the Jacobi angle γ, and $\hat{l}$ is the orbital angular momentum operator. The quantity, μ is the three-body scaled reduced mass (calculated accordingly from the masses of the three atoms involved in the reaction). The BF z-axis is defined to be parallel to $\hat{R}$ and the diatom lies in the (x, z) plane. The quantity $\hat{l}^2$ is expressed as

$$\hat{l}^2 \equiv (\hat{J} - \hat{j})^2 = \hat{J}^2 + \hat{j}^2 - 2\hat{J}_z\hat{j}_z - \hat{J}_+\hat{j}_- - \hat{J}_-\hat{j}_+, \tag{4}$$

where $\hat{J}$ is the total angular momentum operator and $\hat{J}_z$ and $\hat{j}_z$ are the respective BF z components of $\hat{J}$ and $\hat{j}$. $\hat{J}_+(\hat{J}_-)$ and $\hat{j}_+(\hat{j}_-)$ are the corresponding raising (lowering) operators. Within the CS [30] approximation the last two terms of Eq. (4) are neglected. The elements of the diabatic electronic Hamiltonian matrix of Eq. (2) are obtained by diabatizing the adiabatic electronic Hamiltonian matrix through the following similarity transformation:

$$\begin{pmatrix} U_{11} & U_{12} \\ U_{21} & U_{22} \end{pmatrix} = S\begin{pmatrix} V_- & 0 \\ 0 & V_+ \end{pmatrix}S^{\dagger} \tag{5}$$

$$= \frac{V_- + V_+}{2}\mathbf{1} + \frac{V_+ - V_-}{2}$$

$$\times \begin{pmatrix} -\cos\chi & \sin\chi \\ \sin\chi & \cos\chi \end{pmatrix} \tag{6}$$

with

$$S = \begin{pmatrix} \cos\phi & \sin\phi \\ -\sin\phi & \cos\phi \end{pmatrix}. \tag{7}$$

The quantities V_- and V_+ represent the JT-split lower and upper adiabatic sheets of the DMBE PES [31], and S defines the unitary transformation matrix from the adiabatic-to-diabatic representation; $\Psi^{\mathrm{diab}} = S\Psi^{\mathrm{adiab}}$; ϕ is the adiabatic-to-diabatic mixing angle. The quantity $\chi(=2\phi)$ above is the pseudorotation angle defined to be the polar angle of the e-type vibration in the two-dimensional vibrational subspace of the system. It has been demonstrated that this scheme of diabatization removes the leading singular derivative coupling of the adiabatic electronic representation and is able to yield quantitative experimental informations [29,30]. At this point it is worthwhile to mention that we have assessed the accuracy of the DMBE PES by performing new *ab initio* calculations in our previous article [27]. The resulting potential energy data

revealed remarkably good agreement with those from the DBME PES [31]. Therefore, the comparison between the coupled and uncoupled surface results presented here are expected to be accurate enough to draw meaningful conclusions.

In the adiabatic representation the electronic part of the Hamiltonian is diagonal and the nonadiabatic coupling elements appear as off-diagonal elements in the nuclear part of the Hamiltonian. The adiabatic Hamiltonian matrix can be obtained from the diabatic one of Eq. (2) through the following similarity transformation:

$$H^{ad} = S^{\dagger} H^{d} S. \tag{8}$$

2.2. Flux operator and reaction probability

The flux operator $\hat{F}$ is defined in terms of a dividing surface Φ which is the function of a suitable coordinate that separates the product from the reactants. In a diabatic electronic basis, this is given by the commutator

$$\hat{F} = \frac{i}{\hbar}[H^{d}, \Phi], \tag{9}$$

where

$$\Phi = h(r - r_{d}). \tag{10}$$

The quantity h above is a heaviside step function which equals unity for a positive argument and zero otherwise. r_{d} is chosen far out in the product channel to ensure the asymptotic motion for all $r = r_{d}$. The reaction probability is the expectation value of the above flux operator in the basis of the energy normalized time-independent reactive scattering wave function evaluated at $r = r_{d}$. We write this wavefunction in the diabatic electronic basis as

$$|\Phi^{d}(R, r_{d}, \gamma, E)\rangle = \begin{pmatrix} |\phi_{1}^{d}(R, r_{d}, \gamma, E)\rangle \\ |\phi_{2}^{d}(R, r_{d}, \gamma, E)\rangle \end{pmatrix}, \tag{11}$$

where ϕ_{1}^{d} and ϕ_{2}^{d} corresponds to the wavefunction components on the diabatic state 1 and 2, respectively. For an initial state i (corresponding to a specific vibrational v and rotational j state of the reagent diatom) the energy resolved reaction probability is given by [27]

$$P_{i}^{R}(E) = \sum_{f} |S_{fi}^{R}|^{2} = \langle \Phi^{d}(R, r_{d}, \gamma, E)|\hat{F}|\Phi^{d}(R, r_{d}, \gamma, E)\rangle \tag{12}$$

$$= \frac{\hbar}{\mu} \sum_{k=1}^{2} \mathrm{Im}\left[\left\langle \phi_{k}^{d}(R, r_{d}, \gamma, E)\left|\frac{\partial \phi_{k}^{d}(R, r_{d}, \gamma, E)}{\partial r}\right\rangle\right]\right|_{r=r_{d}}. \tag{13}$$

The quantity in the right-hand side of the above equation is integrated over the entire range of R and γ. The energy normalized time-independent reactive scattering wavefunction is calculated along the dividing surface at, $r = r_{d}$ by

$$|\phi_{k}^{d}(R, r_{d}, \gamma, E)\rangle = |\psi_{k}^{d}(R, r_{d}, \gamma, E)\rangle/\kappa_{E}. \tag{14}$$

The function $\psi_{k}^{d}(R, r_{d}, \gamma, E)\rangle$ is obtained by Fourier transforming the time-evolved WP $\psi_{k}^{d}(R, r_{d}, \gamma, t)\rangle$ along the dividing surface

$$|\psi_{k}^{d}(R, r_{d}, \gamma, E)\rangle = \frac{1}{\sqrt{2\pi}} \int_{-\infty}^{+\infty} e^{iEt/\hbar} |\psi_{k}^{d}(R, r, \gamma, t)\rangle dt\big|_{r=r_{d}}. \tag{15}$$

The quantity κ_{E} in Eq. (14) is the weight of the translational component $F(R)$ contained in the initial WP for a given total energy E

$$\kappa_{E} = \left(\frac{\mu}{2\pi\hbar k}\right)^{1/2} \int_{-\infty}^{+\infty} F(R)e^{ikR} dR, \tag{16}$$

where $k = \sqrt{2\mu(E - \epsilon_{vj})}/\hbar$, with ϵ_{vj} being the initial rovibrational energy of the reagent molecule. For the present two state problem, the flux operator in the adiabatic electronic basis depends (see Ref. [27] for details) only on the reaction coordinate (here r), so only the r-dependent part of the nuclear kinetic energy operator is of relevance in Eq. (9). The nuclear kinetic energy operator of the Hamiltonian in this basis is nondiagonal and consequently the flux operator possesses nondiagonal elements. We redefine the energy normalized time-independent reactive scattering wavefunction in the adiabatic electronic basis as

$$|\Phi^{ad}(R, r_{d}, \gamma, E)\rangle = \begin{pmatrix} |\phi_{-}^{ad}(R, r_{d}, \gamma, E)| \\ |\phi_{+}^{ad}(R, r_{d}, \gamma, E)\rangle \end{pmatrix}, \tag{17}$$

where ϕ_{-}^{ad} and ϕ_{+}^{ad} represent the two components of this wavefunction on V_{-} and V_{+}, respectively. The reaction probability in the adiabatic electronic representation is then given by [27]

$$P_{i}^{R}(E) = \frac{\hbar}{\mu}\left[\mathrm{Im} < \phi_{-}^{ad}(R, r_{d}, \gamma, E)|\frac{\partial \phi_{-}^{ad}(R, r_{d}, \gamma, E)}{\partial r} >\right]$$
$$+ \frac{\hbar}{\mu}\left[\mathrm{Im} < \phi_{+}^{ad}(R, r_{d}, \gamma, E)|\frac{\partial \phi_{+}^{ad}(R, r_{d}, \gamma, E)}{\partial r} >\right]$$
$$+ \frac{\hbar}{\mu}\left[2\mathrm{Im} < \phi_{-}^{ad}(R, r_{d}, \gamma, E)|\frac{\partial \phi_{+}^{ad}(R, r_{d}, \gamma, E)}{\partial r} >\right]. \tag{18}$$

The probability expression in the adiabatic electronic basis, therefore, contains the off-diagonal electronic contributions in contrast to the same (Eq. (13)) in a diabatic electronic basis.

2.3. Reaction cross section and thermal rate constant

The cumulative reaction probability for a given initial (v, j) state is calculated by summing up the reaction probability results for different partial wave contributions as follows [32]:

$$N_{vj}(E) = \sum_{\Omega=0}^{j} \frac{g_{\Omega}}{(2j+1)} \sum_{J \geqslant \Omega}^{J_{max}} (2J+1)P_{vj}^{J\Omega}(E), \tag{19}$$

where the quantity g_{Ω} is the degeneracy factor; $g_{\Omega} = 1$ for $\Omega = 0$, and $g_{\Omega} = 2$ for $\Omega \neq 0$. The total reaction cross section is given by

$$\sigma_{vj}(E) = \frac{\pi}{k^2} N_{vj}(E). \tag{20}$$

The initial state-selected thermal rate constant can be obtained from the total reaction cross section [33] as

$$K_{vj}(T) = \sqrt{\frac{8K_{\mathrm{B}}T}{\pi\mu}} \frac{1}{(K_{\mathrm{B}}T)^2} \int_0^\infty E\sigma_{vj}(E)\mathrm{e}^{-E/K_{\mathrm{B}}T}\,\mathrm{d}E, \tag{21}$$

where K_{B} is the Boltzmann constant. Finally, the rotationally averaged thermal rate constants can be obtained by averaging over a Boltzmann distribution of such states

$$K_v(T) = \sum_j \frac{K_{vj}(E)}{Q_{\mathrm{rot}}}(2j+1)\mathrm{e}^{-Bj(j+1)hc/K_{\mathrm{B}}T}, \tag{22}$$

where B is the rotational constant of the reagent and Q_{rot} is the rotational partition function given by

$$Q_{\mathrm{rot}} = \sum_j (2j+1)\mathrm{e}^{-Bj(j+1)hc/K_{\mathrm{B}}T}. \tag{23}$$

3. Computational details

In this section we describe the calculation of reaction probabilities, cross sections and thermal rate constants of the system using the formalism described above in Section 2. The TDSE [Eq. (1)] is solved numerically on a grid in the (R, r, γ) space using the matrix Hamiltonian of Eq. (2). In a reactive scattering study the initial wavefunction is prepared in the asymptotic reactant channel where the interaction potential almost vanishes. In such a situation the initial wavefunction pertinent to the reacting system can be written as a product of the translational wavefunction $F(R)$ for the motion along R and the rovibrational wavefunction Φ_{vj} of the reagent molecule. We locate the wavefunction initially on the repulsive lower adiabatic sheet (V_-) of the DMBE PES which assumes the form

$$|\Psi^J_\Omega(R_l, r_m, \gamma_n, t=0)\rangle = \sqrt{\omega_n} F(R_l)\phi_{vj}(r_m)\tilde{P}^\Omega_j(\cos\gamma_n), \tag{24}$$

where R_l, r_m and γ_n are the grid points in the (R, r, γ) space. The quantity Ω is the quantum number for the projection of j (and also J) on the BF z-axis and; $-\min(j,J) \leqslant \Omega \leqslant \min(j,J)$. We choose a minimum uncertainty Gaussian wave packet (GWP) for $F(R)$:

$$F(R) = \left(\frac{1}{2\pi\delta^2}\right)^{\frac{1}{4}} \exp\left[-\frac{(R-R_0)^2}{4\delta^2} - \mathrm{i}k_0(R-R_0)\right]. \tag{25}$$

The quantity δ is the width parameter of the GWP, and R_0 and k_0 correspond to the location of its maximum in the coordinate and momentum space, respectively. The functions ϕ_{vj} represent the rovibrational eigenfunctions corresponding to a vibrational v and rotational j states of the reagent molecule. We have used the sine discrete variable (sine-DVR) representation approach of Colbert and Miller [34] to solve the rovibrational eigenvalue equation for ϕ_{vj}:

$$\left[-\frac{\hbar^2}{2\mu'}\frac{d^2}{dr'^2} + V(r') + \frac{j(j+1)\hbar^2}{2\mu'r'^2}\right]\phi_{vj}(r') = \epsilon_{vj}\phi_{vj}(r'). \tag{26}$$

Here μ' is the reduced mass, ϵ_{vj} the energy eigenvalue, $r' = r(\mu/\mu')^{1/2}$, the unscaled internuclear distance of the reagent molecule. $V(r')$ is its potential energy obtained from the DMBE PES [31] by setting $R \to \infty$. The initial wavefunction defined in Eq. (24) is transformed to the diabatic electronic representation by using the S matrix (Eq. (7)) prior to the propagation. In the diabatic electronic representation the initial wavefunction can be written in the vector notation as

$$\Psi^{\mathrm{d}}(R, r, \gamma, t=0) = \psi^{\mathrm{d}}_1(R, r, \gamma, t=0)\begin{pmatrix}1\\0\end{pmatrix} + \psi^{\mathrm{d}}_2(R, r, \gamma, t=0)\begin{pmatrix}0\\1\end{pmatrix}, \tag{27}$$

where $\begin{pmatrix}1\\0\end{pmatrix}$ and $\begin{pmatrix}0\\1\end{pmatrix}$ indicate the first and the second diabatic electronic state with energy U_{11} and U_{22}, respectively. The time axis is divided into N segments of length Δt and the exponential time evolution operator of Eq. (1) at each time step is then approximated by the chebychev polynomial expansion method [35] as

$$\exp[-\mathrm{i}\hat{H}\Delta t/\hbar] = \exp(-\mathrm{i}\overline{H}\Delta t/\hbar)\exp(-\mathrm{i}\alpha\hat{H}_{\mathrm{norm}}), \tag{28}$$

where $\hat{H}_{\mathrm{norm}} = 2(\hat{H} - \overline{H})/\Delta E$, with, $\overline{H} = (E_{\max} + E_{\min})/2$, and, $\Delta E = E_{\max} - E_{\min}$. H_{norm} represents the scaled Hamiltonian operator with eigenvalues in $(-1,1)$. The fast Fourier transformation method (FFT) [36] is used to evaluate the action of the radial kinetic energy operators on the wavefunction, where as, the action of the angular kinetic energy operator is evaluated by a discrete variable representation (DVR) [37] method.

The grid along R and r consists of equally spaced points and the grid along γ is constructed for each value of Ω. For the latter purpose, the matrix of the $\cos\gamma$ operator in the basis of the associated Legendre polynomials is diagonalized. The resulting diagonal elements define the nodes of a n-point Gauss Legendre quadrature [38] and the DVR to the finite basis representation (FBR) transformation matrix is given by the eigenvector matrix U. The quadrature weight associated with the grid points are calculated by $w_n^{1/2} = \sqrt{\frac{2^{K+1}K!}{(2K+1)!!}}\sin^{-K}(\gamma_n)U_{1n}$, where U_{1n} refers to the first row of U (the lowest value of j, i.e., $j = \Omega$). The action of the rotational kinetic energy operator is then carried out by transforming the DVR wavefunction to the angular momentum space (FBR), multiplying it by the diagonal value of the angular kinetic energy operator, and transforming it back to the DVR representation. To avoid unphysical reflections or wrap arounds at the grid boundaries, the WP at each time step is multiplied by a damping function [39]

$$f(X_i) = \sin\left[\frac{\pi}{2}\frac{(X_{\mathrm{mask}} + \Delta X_{\mathrm{mask}} - X_i)}{\Delta X_{\mathrm{mask}}}\right], \quad X_i \geqslant X_{\mathrm{mask}} \tag{29}$$

which is activated in the asymptotic reactant and product channels. X_{mask} is the point at which the damping function is initiated and $\Delta X_{\mathrm{mask}}(=X_{\max} - X_{\mathrm{mask}})$ is the width of X

Table 1
Numerical grid parameters and properties of the initial wavefunction used in the present study

Parameter	Value	Description
$N_R/N_r/N_\gamma$	128/64/48	Number of grid points
R_{min}/R_{max} (a_0)	0.1/15.34	Extension of the grid along R
r_{min}/r_{max} (a_0)	0.5/8.06	Extension of the grid along r
$\Delta R/\Delta r$ (a_0)	0.12/0.12	Grid spacings along R and r
r_d (a_0)	4.10	Location of the dividing surface in the product channel
R_{mask}/r_{mask} (a_0)	11.74 /4.70	Starting point of the masking function
R_0 (a_0)	10.5	Initial location of the center of the GWP in the coordinate space
E_{trans} (eV)	2.0	Initial translational kinetic energy
δ (a_0)	0.16	Initial width parameter of the GWP
Δt (fs)	0.135	Length of the time step used in the WP propagation
T (fs)	413.76	Total propagation time

over which the function decays from 1 to 0, with X_{max} being the maximum value of X in that direction. The properties of the initial WP and the grid parameters used for the numerical calculations are listed in Table 1.

We here note that the three particle permutation symmetry in case of H + H₂ collision is not incorporated in the present formalism. It is shown in Ref. [22] that if necessary this symmetry can be included after the calculation. The purpose of this paper is to examine the effect of the upper surface on the nuclear dynamics and to compare the findings with the GP results from the current literature obtained by excluding this symmetry effects [22]. We also mention that this symmetry effect is expected to be quite small as revealed by our earlier treatment of the bound states [26] of the upper adiabatic surface and subsequent comparison with the GP results from the literature [45].

4. Results and discussion

In this section, we present and discuss the reaction probability, reaction cross section and thermal rate constant results obtained for the H + H₂ and H + HD exchange reactions, employing the theoretical and computational details illustrated above. The reaction probabilities are calculated upto the three-body dissociation limit of ∼4.74 eV. In the CS model inclusion of partial-wave contributions upto $J = 50$ in case of H + H₂ and 60 in case of H + HD, respectively, are found to be necessary to obtain converged cross section results in this energy range both in the coupled and uncoupled surface calculations. The convergence of each calculation is checked with respect to the choice of the numerical grid parameters given in Table 1. A more exact treatment of the dynamics including the coriolis coupling terms is beyond the scope of the present article and will be addressed in a forthcoming publication.

4.1. Reaction probability and time dependence of electronic population

The H + H₂ $(v = 0, \ j = 0) \rightarrow$ H₂$(\sum v', \sum j')$ + H reaction probability values as a function of the total energy E (H, H₂ translational + H₂ rovibrational) are plotted in

Fig. 1a for a few selected values of the total angular momentum, $J = 0, 10, 20, 30, 40$ and 50 (indicated in the panel) and for $\Omega = 0$. These represent the initial state selected and energy resolved total (summed over all open v' and j' levels of the product H₂ at a given energy) reaction probabilities. The coupled and uncoupled surface results are shown by the solid and dashed lines, respectively. The reaction probabilities in both cases are calculated for the entire relevant energy range starting from the onset of the reaction to the three body break-up limit of
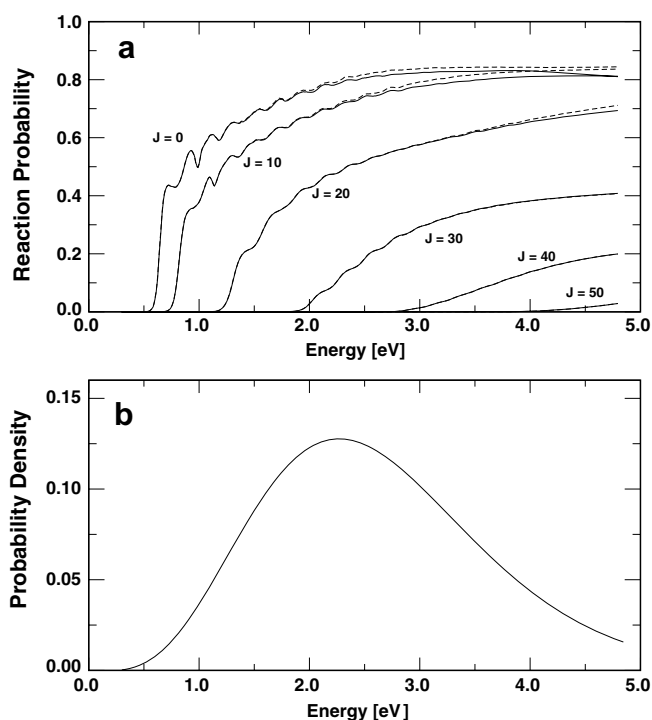

Fig. 1. (a) Total reaction probabilities as a function of the total energy E (H, H₂ translational + H₂ rovibrational) for the H + H₂ $(v = 0, \ j = 0) \rightarrow$ H₂$(\sum v', \sum j')$ + H exchange reaction on the DBME PES for the total angular momentum, $J = 0, 10, 20, 30, 40$ and 50 (indicated in the panel). The coupled and uncoupled surface results are shown by the solid and dashed lines, respectively. The zero of the energy scale corresponds to infinitely separated reagent. (b) The energy distribution of the initial translational (H, H₂) GWP used for calculating the above reaction probabilities.

$\sim$4.74 eV. The initial WP is prepared in the asymptotic reagent channel of the lower adiabatic sheet (V_-) of the DMBE PES. The energy distribution of the translational GWP is shown in Fig. 1b. It can be seen from Fig. 1b that the translational energy components of the initial GWP cover a broad range of energies which fits well to the energy range examined here. We note here that, this is the first theoretical work of its kind which considers to investigate this exchange reaction over such a wide range of energy. It can be seen from Fig. 1a that the reaction onset in both the coupled and uncoupled state situation shifts to higher energies with an increase in the total angular momentum, J. The resonance structures and their energetic locations remain same for a given value of J in the coupled and uncoupled surface situations. The difference between the coupled and uncoupled surface reaction probabilities for a given value of J is nearly zero at low energies. At higher energies near and above the energetic minimum of the seam of CIs (at $\sim$2.74 eV) this difference becomes noticeable (cf., Fig. 1a). However, as J increases, the coupled and uncoupled surface results merge on each other, particularly for $J \geqslant 30$. The resonance structures seen in the reaction probability curves at low J values gradually disappear as J increases. Beyond $J = 40$ these resonances are not at all seen in the reaction probability curves.

The effect of rotational and vibrational excitation of the reagent H_2 on the coupled and uncoupled surface reaction probabilities of the $H + H_2$ reaction is shown in Fig. 2a and b, respectively. In Fig. 2a, the reaction probabilities of the reagent H_2 ($v = 0$, $j = 1$–3) for $J = 10$ and $\Omega = 0$

are plotted. Again, the coupled and uncoupled surface results are shown by the full and dashed lines, respectively. It can be seen from Fig. 2a that the difference between the coupled and uncoupled surface results is small at low energies and this difference increases with increasing energies for a given value of j. In addition, with rotational excitation of reagent H_2, the difference between the coupled and uncoupled surface results increases and for $j = 3$, it becomes quite substantial already at energies much below the minimum of the seam of CIs. As the initial rotation of the reagent H_2 correlates with the internal rotation of the system around the CI, it is possible for the nuclear wavefunction to encircle the CI on the lower adiabatic sheet even if the upper one is not accessible at these energies. Therefore, the nonadiabatic effects seen in the reaction probability curve for $j = 3$ are likely to arise from the geometric phase. In Fig. 2b we show the reaction probabilities of the reagent H_2 ($v = 1$–3, $j = 0$) for $J = 10$ and $\Omega = 0$. The onset of the reaction shifts to higher energies with the vibrational excitation of the reagent H_2. The coupled and uncoupled surface results are shown in the panel by the full and the dashed lines, respectively. For a given value of v, the difference between the coupled and the uncoupled surface results is small at low energies and it increases slightly with an increase in the energy. This slight difference is more visible beyond the energetic minimum of the seam of CIs. As the vibrational quantum number increases, the difference between the coupled and the uncoupled surface results also increases slightly. However, the effect of the nonadiabatic coupling on the reaction dynamics with reagent vibrational excitation appears not very significant.

In Fig. 3, the J dependence of the degeneracy ($2J + 1$) weighed reaction probability for the $H + H_2$ ($v = 0$, $j = 0$) reaction for eight representative values of the total energy (indicated in the panel) calculated from the probability results obtained in the coupled surface situation are shown. This analysis helps to assess the partial wave contributions to the integral reaction cross sections (discussed later in the text) for a given value of the total energy. The weighed probability value for a given energy initially increases with J due to the ($2J + 1$) degeneracy factor and then decreases at higher values of J, due to the shift of the reaction threshold caused by the centrifugal barrier. The partial wave contribution increases with increasing total energy, and J values upto 50 are necessary to include to obtain the converged reaction cross sections upto a total energy of $\sim$4.5 eV. The mild oscillations (mostly at low energy values) in the probability curves in Fig. 3 are associated with the resonances of the $H + H_2$ system. These oscillations disappear with an increase in the energy.

In order to better understand the similarities between the coupled and uncoupled surface results we show in Fig. 4 the time evolution of the electronic populations in the coupled surface dynamics of $H + H_2$ ($v = 0$, $j = 0$) reaction for different values of J and $\Omega = 0$. The initial WP is prepared in the reagent asymptote of the lower adiabatic sheet of the DMBE PES. It is transformed to the diabatic
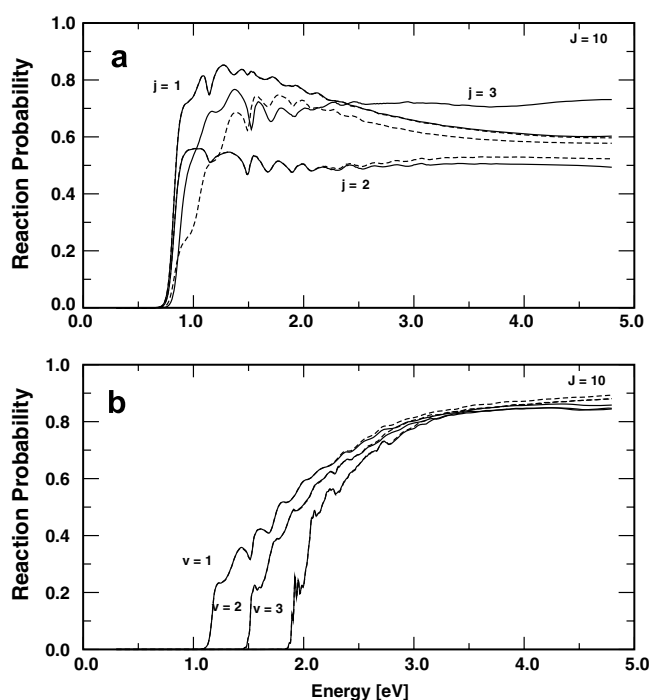

Fig. 2. Same as in Fig. 1a for (a) $H + H_2$ ($v = 0$, $j = 1$–3) $\rightarrow H_2$ ($\sum v'$, $\sum j'$) + H and (b) $H + H_2$ ($v = 1$–3, $j = 0$) $\rightarrow H_2$ ($\sum v'$, $\sum j'$) + H and for $J = 10$, $\Omega = 0$.
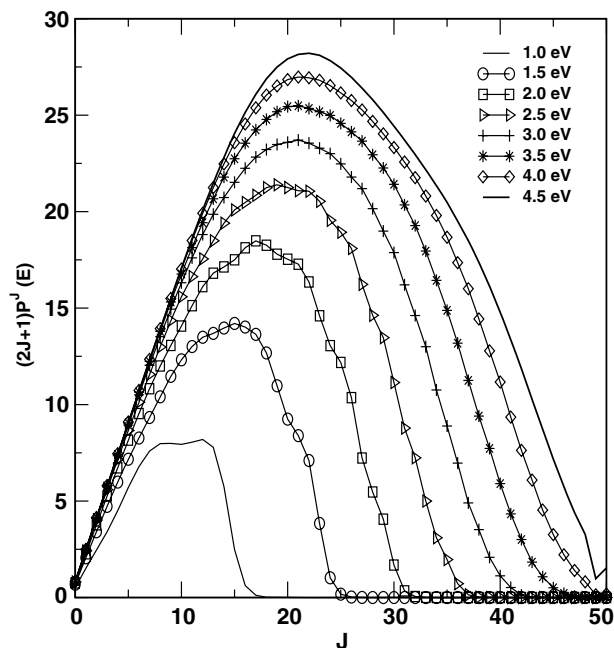
Fig. 3. Weighted partial wave contribution to the integral reaction cross sections at various values of the total energy (indicated in the panel) for the H + H$_2$ ($v = 0$, $j = 0$) reaction.

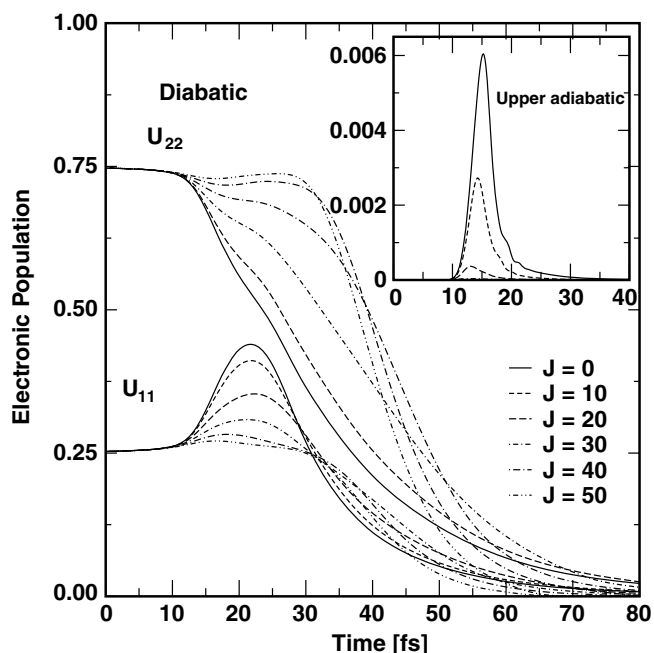Fig. 4. Electronic population dynamics for the H + H$_2$ ($v = 0$, $j = 0$) → H$_2$ ($\sum v'$, $\sum j'$) + H exchange reaction. The population of two component diabatic electronic states U_{11} and U_{22} for various values of the total angular momentum, J are shown by different line types (indicated in the panel). Because of the damping function activated at the grid edge, the above populations approach to zero at longer times. The maximum of the time-dependent population of the upper adiabatic electronic state (V_+) for different values of J are shown in the inset of the figure.

electronic representation using the S matrix (cf., Eq. (7)) prior to the propagation. The two component diabatic

populations for different values of J are shown by different line types indicated in Fig. 4. It can be seen from Fig. 4 that the population of the two component diabatic electronic states are ~0.75 and ~0.25 at $t = 0$. Therefore, we note that the asymptotic adiabatic potential also represents an admixture of the two diabatic potentials. However, as discussed in our earlier article [27], this does not introduce any numerical artifact in the dynamical attributes. At longer times (>50 fs) the populations of both diabatic sheets approached zero. This is because of the absorption of the wavepacket at grid edges by the damping function. The WP component reaching the upper adiabatic electronic state during the dynamics is shown in the inset of Fig. 4 for different values of J indicated in the figure. The population of this state reaches a maximum value of ~6×10^{-3} after ~15 fs for $J = 0$. But as J increases, the population of this state decreases. These maximum populations are ~2.7×10^{-3} and ~3.8×10^{-4} for $J = 10$ and 20, respectively. Beyond $J = 20$, the population of this state is found to be almost negligible.

We now discuss the above dynamical quantities calculated for the isotopic H + HD reaction. This reaction yields either HD + H (channel R1) or H$_2$ + D (channel R2) products. Therefore, we in the following consider to show both the channel specific as well as total reaction probabilities. The reaction probability values for H + HD ($v = 0$, $j = 0$) reaction as a function of the total energy E are plotted in Fig. 5a–c for five selected values of the total angular
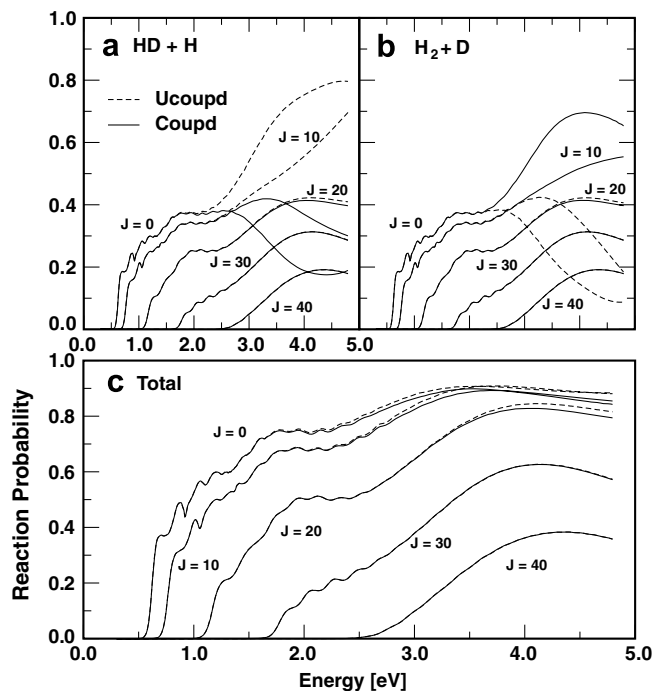

Fig. 5. Reaction probabilities of the H + HD ($v = 0$, $j = 0$) reaction for the (a) H + HD (R1) and (b) H$_2$ + D (R2) channels as a function of total energy, E. The sum total of these probabilities are plotted in panel (c). The probabilities are shown for various values of the total angular momentum, J indicated in each panel.

momentum, $J = 0$, 10, 20, 30 and 40 and for $\Omega = 0$. The reaction probabilities obtained in the uncoupled and coupled surface situations are shown by the dashed and solid lines, respectively. The reaction probabilities for channels R1 and R2 are given in panels (a) and (b), respectively, and the overall reaction probabilities (sum total of the two channel specific probabilities) are given in the panel (c). The effect of the nonadiabatic coupling on the channel specific reaction probabilities of panel (a) and (b) appears to be quite large for $J = 0$ and 10. These reveal a classic signature of nonadiabatic interactions including the geometric phase. Interestingly, the uncoupled and coupled surface results exhibit opposite behaviour beyond the energetic minimum of the seam of CIs for $J = 0$ and 10 as shown in panels (a) and (b) for the R1 and R2 channels, respectively. And for $J = 20$ and beyond the differences between the uncoupled and coupled surface results are negligible. Due to this, the effect of the nonadiabatic interactions averages out in the total reaction probability results of panel (c) for small values of J. This may be because the inelastic probability $(1 -$ total reaction probability) is not expected to show any geometric phase effects as it would require the nuclear wavefunction to traverse infeasible paths over three transition states. A verification of this will be worthwhile and will be addressed in a future publication. For large J values, the channel specific reaction probabilities seem not to be affected by the nonadiabatic coupling and therefore, a similar trend is also observed in the total reaction probability results.

It emerges from the above discussion that the nonadiabatic coupling have almost similar effects in the H + H$_2$ and H + HD reaction dynamics. At a more detailed level the channel specific reaction probabilities of the latter are seen to be severely affected by this coupling for low J values. A similar analysis to that depicted in Fig. 3 for the H + H$_2$ reaction revealed that the partial wave contributions upto $J = 60$ are necessary to obtain converged integral reaction cross sections for H + HD reaction upto the three-body dissociation limit.

4.2. Initial state-selected integral reaction cross sections

The initial state-selected and energy resolved integral reaction cross sections, as a function of the total energy in the H + H$_2$ collisions are shown in Fig. 6a–d. These cross sections are calculated by Eq. (20). The coupled and uncoupled surface results are shown by the full and dashed lines, respectively, in each panel. The reaction cross sections shown in Fig. 6a–d for both the coupled and uncoupled surface situations are obtained with the rotationally excited reagent H$_2$ ($j = 0$–3, in panels (a)–(d), respectively) in the vibrational ground level ($v = 0$). The cross section results for $j > 0$ includes the contributions from $\Omega > 0$ and as stated above, $\Omega_{max} = \min(j, J)$, within the CS approximation. For a given value of j the reaction cross section increases with energy reaching a maximum in the energy range of $\sim$2.5–2.7 eV and then decreases as the energy increases in both the coupled and uncoupled
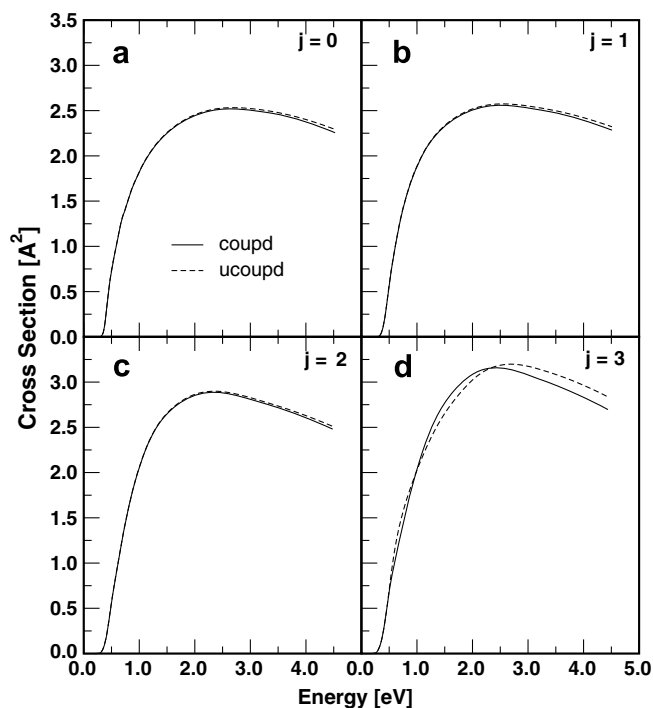

Fig. 6. Initial state-selected integral reaction cross sections of the H + H$_2$ ($v = 0$, j) as a function of the total energy. The cross sections for various j values are indicated in each panel.

surface results. The difference between the coupled and the uncoupled surface results for a given value of j, is small at low collision energies and increases very slightly for $j = 0$–2 beyond the energetic minimum of the seam of CIs. This difference appears to be somewhat larger for $j = 3$. The results of Fig. 6 do not reveal any dramatic effect of nonadiabatic coupling in the H + H$_2$ reaction dynamics in par with the recent GP results. The integral reaction cross sections obtained with vibrationally excited H$_2$ are shown in Fig. 7a–d for $v = 0$–3, respectively. In this case also no dramatic effect of the nonadiabatic coupling can be observed. The coupled surface results (solid lines) remain essentially identical to the uncoupled surface (dashed lines) results.

The initial state-selected total integral reaction cross sections for the H + HD ($v = 0$, $j = 0$–3) reaction are plotted in Fig. 8a–d as a function of total energy. Unlike H + H$_2$ reaction cross sections (cf., Fig. 6) the H + HD reaction cross sections reveal resonance structures. The difference between the uncoupled (dashed lines) and coupled (solid lines) surface results in this case is somewhat larger when compared to the H + H$_2$ (cf., Fig. 6a–d) results. The trend observed in the channel specific reaction probability results (cf., Fig. 4a–c) also show up in the channel specific reaction cross sections. The channel specific reaction cross sections are shown for H + HD ($v = 0$, $j = 0$–3) reaction in Figs. 9a and b and 10a and b for the R1 and R2 channels, respectively, for illustration. However, in the total reaction cross section (sum total of R1 and R2 channels) the two opposite trends cancel out and therefore the coupled and uncoupled
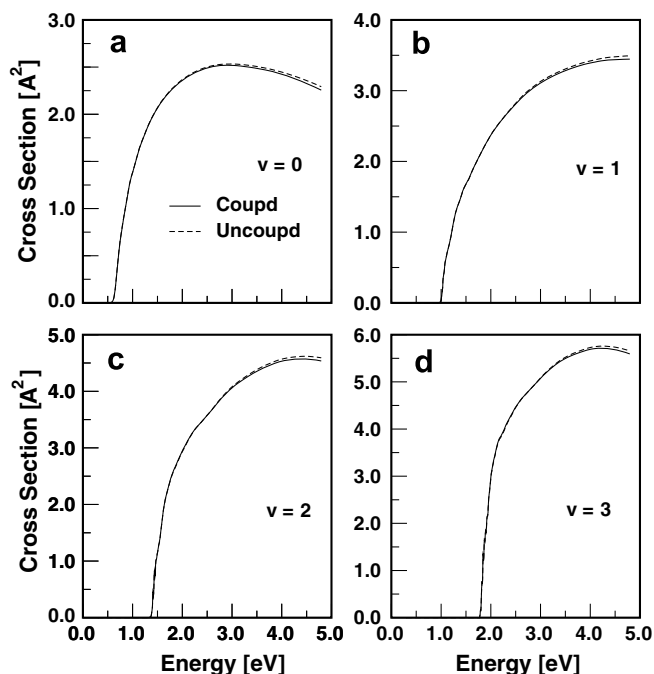
Fig. 7. Same as in Fig. 6, for H + H₂ ($v, j = 0$) reaction. The cross sections for various v values are indicated in each panel.
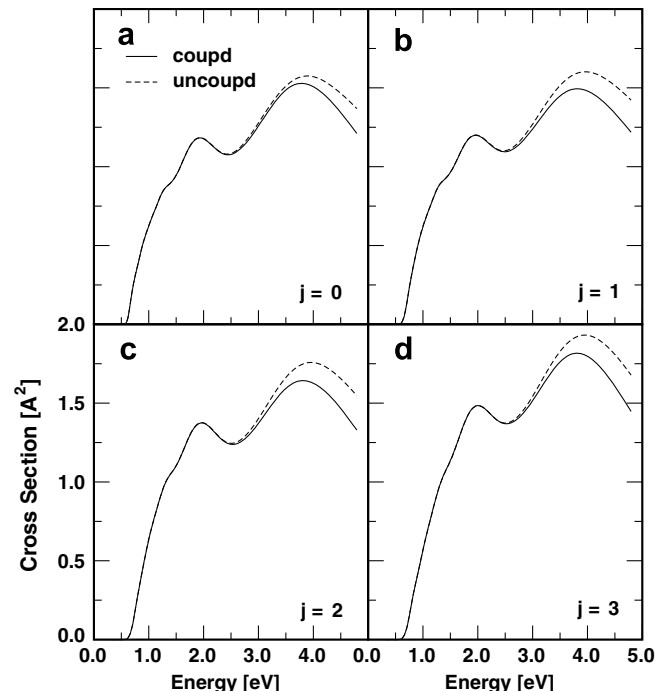

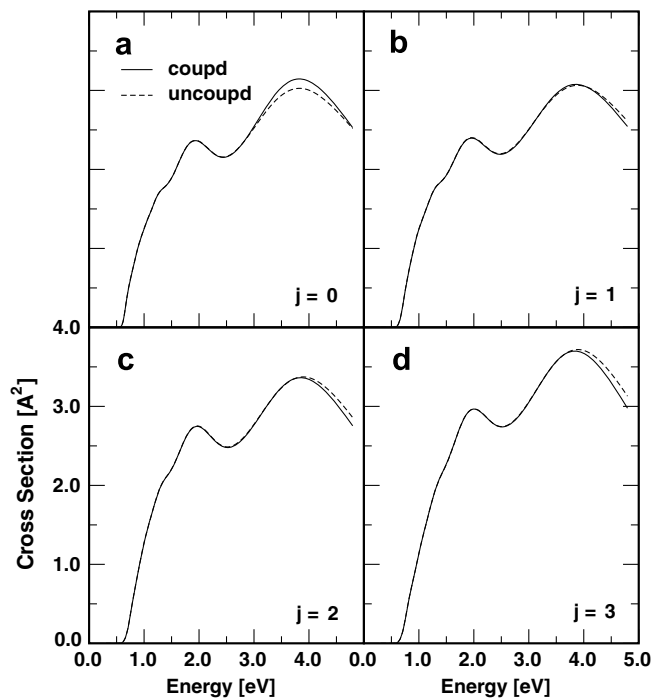Fig. 9. Same as in Fig. 8 for HD + H channel of H + HD ($v = 0$, j) reaction.

Fig. 8. Same as in Fig. 6 for H + HD ($v = 0$, j) reaction. The cross sections here represent the sum total of those for the HD + H and H₂ + D channels shown for various j values indicated in each panel.
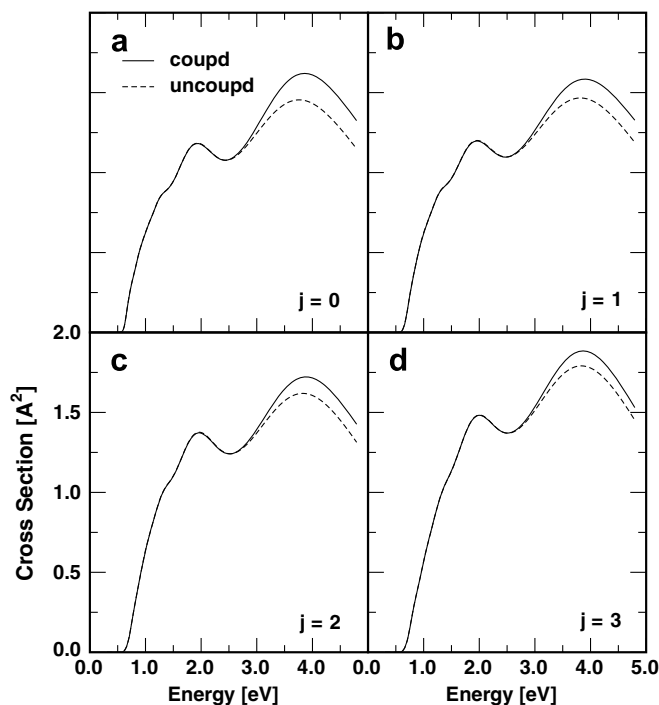

Fig. 10. Same as in Fig. 8 for H₂ + D channel of H + HD ($v = 0$, j) reaction.

surface results essentially becomes identical. The reaction cross section values shown in Fig. 8 differ only after the energetic minimum of CIs. The reaction cross sections obtained with the vibrationally excited HD molecule in the ground rotational level also reveal similar characteristics and are not shown here.

4.3. Thermal rate constants

The thermal rate constants obtained by statistically averaging over the rotational states $j = 0$–3 are shown in Fig. 11 for the H + H₂ ($v = 0$) reaction. The coupled and
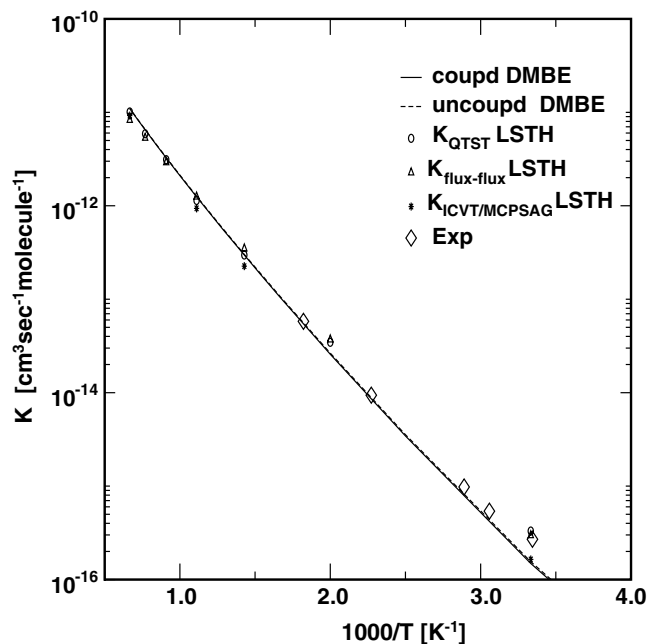
Fig. 11. Arrhenius plot of the Boltzmann averaged (over $j = 0$–3) thermal rate constants for the H + H$_2$ ($v = 0$) reaction. The coupled and uncoupled surface results are shown by solid and dashed lines, respectively. Points on the diagram represents the results from the literature (K_{QTST} LSTH from Ref. [39]; $K_{flux-flux}$ LSTH from Ref. [40]; $K_{ICVT/MCPSAG}$ LSTH from Ref. [41]. The experimental values are taken from the Table IX of Ref. [39]).

Fig. 12. Same as in Fig. 9 for H + HD ($v = 0$) reaction. Thermal rate constants for the HD + H and H$_2$ + D channels are shown in panel (a) and (b), respectively. The points on the diagram refer to the results from the Ref. [42].

uncoupled surface results are shown by the full and dashed lines, respectively. The rate constants values available in the literature are shown by different points on the diagram. The meaning of various points are also indicated in the panel. The unfilled diamonds represents the experimental points extracted from Table 9 of Pack et al. [41]. With quite minor deviations all results of Fig. 9 are consistent with each other. The minor deviations represent estimates of the accuracy of the PES and the theoretical methods. The present rate constants reveal the expected Arrhenius behaviour. Now most importantly Fig. 11 reveals that the difference between the coupled and uncoupled surface results is insignificant (within the drawing accuracy) in the reported temperature range of ∼0–1500 K. This drives us to the final point of concluding that the important dynamical observable like the thermal rate constant derived from the microscopic reaction probabilities is insensitive to the nonadiabatic coupling in the H + H$_2$ reaction dynamics. Even though, the latter show some effects of coupling in their detailed variations over the considered energy range.

In Fig. 12a and b, we show the thermal rate constants obtained by statistically averaging over the rotational states $j = 0$–3 for the R1 and R2 channels of the H + HD reaction, respectively. The coupled and uncoupled state results are shown by the full and dashed lines, respectively. The difference between the coupled and uncoupled surface results is also insignificant in these cases, although the channel specific reaction cross sections reveal some variations (cf., Figs. 9a–d and 10a–d). The difference apparently
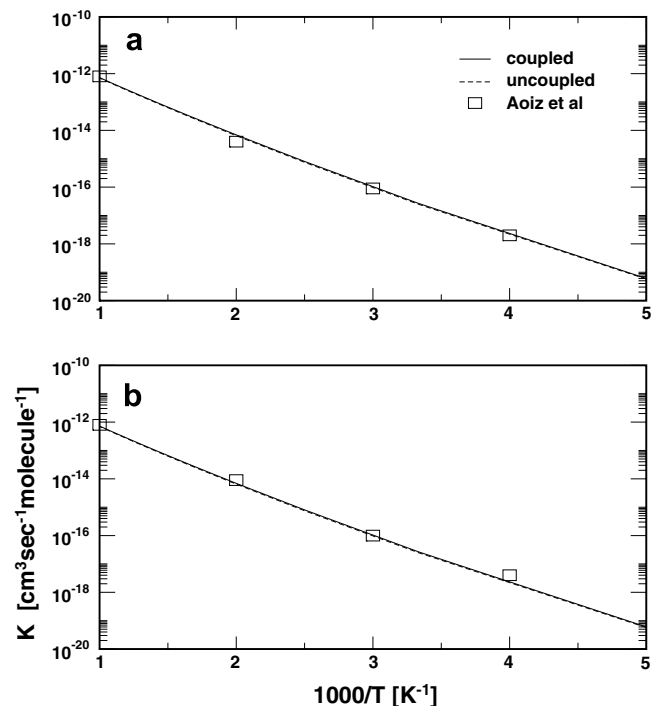
averages out on integrating the cross sections over the energy, to calculate the thermal rate constants. The theoretical results of Aoiz and co-workers extracted from Ref. [43] are superimposed on Fig. 12a and b and are shown as squares. We see that our rate constant values are in good
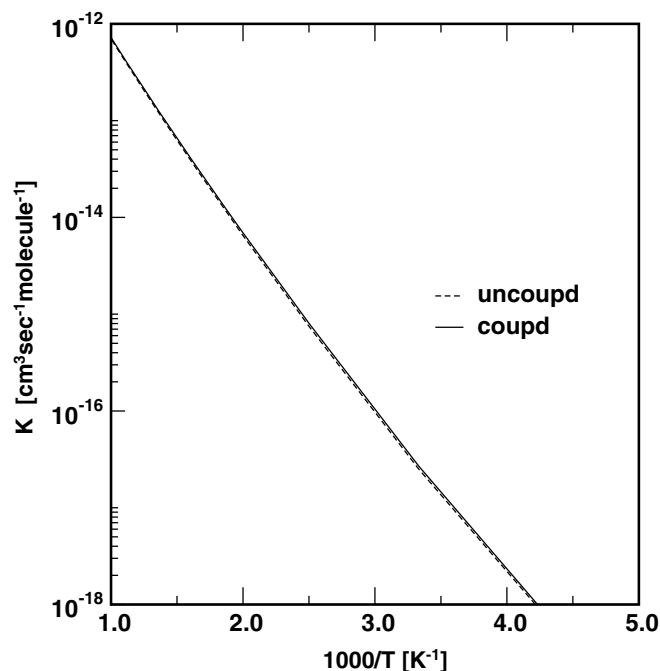

Fig. 13. Same as in Fig. 9, for the total H + HD reaction.

agreement with those of Aoiz and co-workers [43]. In Fig. 13 the total (sum of two channels) thermal rate constants obtained by statistically averaging over the reagent rotational states $j = 0–3$ are shown. Again, the coupled and uncoupled surface results shown by the full and dashed lines, respectively, reveal hardly any difference. We can see from the figure that the difference between the coupled and uncoupled surface results is small in the temperature range considered.

5. Summary

We presented a theoretical account of the electronic nonadiabatic coupling effects on the dynamics of $H + H_2$ (HD) reactions. The $H + H_2$ reaction occurs on the lower adiabatic sheet of its JT-split degenerate ground electronic manifold. The quantum dynamical simulations are carried out by constructing suitable diabatic electronic states and by a time-dependent WP propagation approach within the CS approximation. Calculations of quantum dynamical quantities *e.g.,* initial state-selected energy resolved total reaction probabilities, integral reaction cross sections and thermal rate constants are carried out both in the uncoupled and coupled surface situations in order to explicitly examine the effect of surface coupling on the reaction dynamics.

The quantum dynamical results of both the reactions reveal only minor impact of the nonadiabatic coupling on them. The effect of the surface coupling shows up only beyond the energetic minimum of the seam of conical intersections. Even though the reaction probability results show some sensitivity to this coupling (quite substantial in the channel specific reaction probabilities and reaction cross sections of $H + HD$ reaction, cf., Figs. 5a and b and 8a–d), the effect averages out in the total integral reaction cross sections with inclusion of the contributions from many partial waves. The Boltzmann averaged thermal rate constants are found to be essentially same in the uncoupled and coupled surface situations for both the reactions. The investigations reported in this paper are extended to a wide energy range starting from the onset of the reaction to the three-body dissociation limit. The findings of this paper are in general agreement with the recent literature data obtained by including the GP effect only. We reiterate that the seam of CIs in H_3 occurs at the D_{3h} configuration whereas, the minimum energy path for the reactive scattering occurs at the collinear geometry, and this is perhaps the main reason that no dramatic surface coupling effect can be seen in the dynamics of this prototypical reaction. To this end we mention that the CS approximation is accurate enough for the title reaction. Inclusion of coriolis coupling does not dramatically change the integral reaction cross sections, it only alters very slightly the trend of variation of the reaction cross sections with reagent rotational excitation as noted in a recent publication [44]. Additionally, in a most recent work the GP effects on the coriolis coupling terms are predicted to be very small [22]. Therefore, the general findings of this article are expected to remain same on inclusion of the coriolis coupling terms in the dynamics.

References

[1] F. Fernández-Alonso, R.N. Zare, Ann. Rev. Phys. Chem. 53 (2002) 67;
F.J. Aoiz, L. Bañares, V.J. Herrero, Int. Rev. Phys. Chem. 24 (2005) 119.
[2] D.E. Manolopoulos, R.E. Wyatt, J. Chem. Phys. 92 (1990) 810.
[3] J. Chang, N.J. Brown, J. Chem. Phys. 103 (1995) 4097.
[4] D.M. Charutz, I. Last, M. Baer, J. Chem. Phys. 106 (1997) 7654.
[5] L. Bañares, F.J. Aoiz, V.J. Herrero, M.J. D'Mello, B. Niederjohann, K. Seekamp-Rahn, E. Wrede, L. Schnieder, J. Chem. Phys. 108 (1998) 6160.
[6] S. Sukiasyan, H.D. Meyer, J. Chem. Phys. 116 (2002) 10641.
[7] A. Jäckle, H.D. Meyer, J. Chem. Phys. 109 (1998) 2614.
[8] B.K. Kendrick, J. Chem. Phys. 114 (2001) 8796.
[9] B.D. Bean, J.D. Ayers, F. Fernández-Alonso, R.N. Zare, J. Chem. Phys. 116 (2002) 6634.
[10] S.C. Althorpe, J. Chem. Phys. 117 (2002) 4623.
[11] S.C. Althorpe, F. Fernández-Alonso, B.D. Bean, J.D. Ayers, A.E. Pomerantz, R.N. Zare, E. Wrede, Nature (London) 416 (2002) 67.
[12] S.A. Harich, D. Dai, C.C. Wang, X. Yang, S.D. Chao, R.T. Skodje, Nature (London) 419 (2002) 281.
[13] S.L. Mielke, K.A. Peterson, D.Q. Schuenke, B.C. Garrett, D.G. Truhlar, J.V. Michael, M.C. Su, J.W. Sutherland, Phys. Rev. Lett. 91 (2003) 063201.
[14] D.X. Dai, C.C. Wang, S.A. Harich, X.Y. Wang, X.M. Yang, S.D. Chao, R.T. Skodje, Science 300 (2003) 1730.
[15] F. Ausfelder, A.E. Pomerantz, R.N. Zare, S.C. Althorpe, F.J. Aoiz, L. Bañares, J.F. Castillo, J. Chem. Phys. 120 (2004) 3255.
[16] G. Herzberg, H.C. Longuet-Higgins, Discuss. Faraday. Soc. 35 (1963) 77.
[17] C.A. Mead, D.G. Truhlar, J. Chem. Phys. 70 (1979) 2284.
[18] C.A. Mead, J. Chem. Phys. 72 (1980) 3839.
[19] B. Lepetit, A. Kuppermann, Chem. Phys. Lett. 166 (1990) 581;
Y.M. Wu, A. Kuppermann, B. Lepetit, Chem. Phys. Lett. 186 (1991) 319;
A. Kuppermann, Y.M. Wu, Chem. Phys. Lett. 205 (1993) 577;
A. Kuppermann, Y.M. Wu, Chem. Phys. Lett. 241 (1995) 229;
A. Kuppermann, Y.M. Wu, Chem. Phys. Lett. 349 (2001) 537.
[20] D.A. Kliner, D.E. Adelman, R.N. Zare, J. Chem. Phys. 95 (1991) 1648.
[21] B.K. Kendrick, J. Chem. Phys. 112 (2000) 5679;
B.K. Kendrick, J. Phys. Chem. A 107 (2003) 6739;
B.K. Kendrick, J. Chem. Phys. 118 (2003) 10502.
[22] J.C. Juanes-Marcos, S.C. Althorpe, J. Chem. Phys. 122 (2005) 204324.
[23] J.C. Juanes-Marcos, S.C. Althorpe, E. Wrede, Science 309 (2005) 1227.
[24] A.J.C. Varandas, H.G. Yu, J. Chem. Soc., Faraday Trans. 93 (1997) 819.

[25] R. Bruckmeier, Ch. Wunderlinch, H. Figger, Phys. Rev. Lett. 72 (1994) 2250.

[26] S. Mahapatra, H. Köppel, J. Chem. Phys. 109 (1998) 1721;
S. Mahapatra, H. Köppel, Phys. Rev. Lett. 81 (1998) 3116;
S. Mahapatra, H. Köppel, Faraday Discuss. 110 (1998) 248;
S. Mahapatra, H. Köppel, Chem. Phys. Lett. 306 (1999) 387.

[27] S. Mahapatra, H. Köppel, L.S. Cederbaum, J. Phys. Chem. A 105 (2001) 2321.

[28] S. Mahapatra, Quantum reaction dynamics on multi-sheeted potential energy surfaces, in: W. Domcke, D.R. Yarkony, H. Köppel (Eds.), Conical Intersections: Electronic Structure, Dynamics and Spectroscopy, World Scientific, Singapore, 2004, p. 555.

[29] A. Thiel, H. Köppel, J. Chem. Phys. 110 (1999) 9371;
H. Köppel, J. Gronki, S. Mahapatra, J. Chem. Phys. 115 (2001) 2377.

[30] R.T. Pack, J. Chem. Phys. 60 (1974) 633;
P. McGuire, D.J. Kouri, J. Chem. Phys. 60 (1974) 2488.

[31] A.J.C. Varandas, F.B. Brown, C.A. Mead, D.G. Truhlar, N.C. Blais, J. Chem. Phys. 86 (1987) 6258.

[32] J.Z.H. Zhang, Theory and Application of Quantum Molecular Dynamics, World Scientific, Singapore, 1999.

[33] F.J. Aoiz, L. Bañares, J.F. Castillo, J. Chem. Phys. 111 (1999) 4013.

[34] D.T. Colbert, W.H. Miller, J. Chem. Phys. 96 (1992) 1982.

[35] H. Tal-Ezer, R. Kosloff, J. Chem. Phys. 81 (1984) 3967.

[36] D. Kosloff, R. Kosloff, J. Comput. Phys. 52 (1983) 35.

[37] J.C. Light, I.P. Hamilton, J.V. Lill, J. Chem. Phys. 82 (1985) 1400;
Z. Bačić, J.C. Light, Ann. Rev. Phys. Chem. 40 (1989) 469.

[38] W.H. Press, B.P. Flannery, S.A. Teukolsky, W.T. Vetterling, Numerical Recipes in Fortran: The Art of Scientifc Computing, second ed., Cambridge University Press, New York, 1986, p. 125.

[39] S. Mahapatra, N. Sathyamurthy, J. Chem. Soc., Faraday Trans. 93 (1997) 773.

[40] Y. Zheng, J. Chem. Phys. 122 (2005) 094316.

[41] T.J. Park, J.C. Light, J. Chem. Phys. 91 (1992) 974.

[42] D.K. Bondi, D.C. Clary, J.N.L. Conner, B.G. Garrett, D.G. Rtuhlar, J. Chem. Phys. 76 (1982) 4986.

[43] F.J. Aoiz, M. Brouard, C.J. Eyles, J.F. Castillo, V.S. Rābanos, J. Chem. Phys. 125 (2006) 144105.

[44] S. Sukiasyan, H.-D. Meyer, J. Chem. Phys. 116 (2002) 10641.

[45] B. Lepetit, Z. Peng, A. Kuppermann, Chem. Phys. Lett. 166 (1990) 572.